



THE UNIVERSITY *of* EDINBURGH

Edinburgh Research Explorer

## Nuclear S-nitrosylation impacts tissue regeneration in zebrafish

**Citation for published version:**

Matrone, G, Jung, SY, Choi, JM, Jain, A, Eastwood Leung, H-C, Rajapakshe, K, Coarfa, C, Rodor, J, Denvir, MA, Baker, AH & Cooke, JP 2021, 'Nuclear S-nitrosylation impacts tissue regeneration in zebrafish', *Nature Communications*. <https://doi.org/10.1038/s41467-021-26621-0>

**Digital Object Identifier (DOI):**

[10.1038/s41467-021-26621-0](https://doi.org/10.1038/s41467-021-26621-0)

**Link:**

[Link to publication record in Edinburgh Research Explorer](#)

**Document Version:**

Peer reviewed version

**Published In:**

Nature Communications

**General rights**

Copyright for the publications made accessible via the Edinburgh Research Explorer is retained by the author(s) and / or other copyright owners and it is a condition of accessing these publications that users recognise and abide by the legal requirements associated with these rights.

**Take down policy**

The University of Edinburgh has made every reasonable effort to ensure that Edinburgh Research Explorer content complies with UK legislation. If you believe that the public display of this file breaches copyright please contact [openaccess@ed.ac.uk](mailto:openaccess@ed.ac.uk) providing details, and we will remove access to the work immediately and investigate your claim.



1 **Title: Nuclear S-nitrosylation impacts tissue regeneration in zebrafish**

2 **Authors:** Gianfranco Matrone 1,2\*, Sung Yun Jung 3,4, Jong Min Choi 3, Antrix Jain 3,  
3 Hon-Chiu Eastwood Leung 5, Kimal Rajapakshe 5, Cristian Coarfa 5, Julie Rodor 1, Martin  
4 Denvir 1, Andrew H Baker 1 and John P Cooke 2.

5 **Affiliations:**

- 6 1. British Heart Foundation Centre for Cardiovascular Science, Queen's Medical Research  
7 Institute, The University of Edinburgh, 47 Little France Cres, EH16 4TJ, Edinburgh, UK.  
8 2. Center for Cardiovascular Regeneration, Department of Cardiovascular Sciences, Houston  
9 Methodist Research Institute, Houston, TX, 77030, USA  
10 3. Mass Spectrometry Proteomics Core, Baylor College of Medicine, Houston, TX, USA.  
11 4. Department of Biochemistry and Molecular Biology, Baylor College of Medicine,  
12 Houston, TX, 77030, USA.  
13 5. Department of Molecular & Cell Biology, Baylor College of Medicine, Houston, TX,  
14 77030, USA.

15

16 \* Corresponding author

17 **Correspondence to:** Gianfranco Matrone, Centre for Cardiovascular Science, Room E3.07,  
18 Queen's Medical Research Institute, University of Edinburgh, 47 Little France Crescent,  
19 Edinburgh EH16 4TJ, United Kingdom. Email: [gianfranco.matrone@ed.ac.uk](mailto:gianfranco.matrone@ed.ac.uk) , Tel: +44  
20 (0)131 242 9334;

21 **Key words:** S-nitrosylation, nuclear protein, Kdm1a, zebrafish, regeneration.

22

23 **Abstract**

24 Despite the importance of nitric oxide signaling in multiple biological processes, its role in  
25 tissue regeneration remains largely unexplored. Here, we provide evidence that inducible  
26 nitric oxide synthase (iNos) translocates to the nucleus during zebrafish tailfin regeneration  
27 and is associated with alterations in the nuclear S-nitrosylated proteome. iNos inhibitors or  
28 nitric oxide scavengers reduce protein S-nitrosylation and impair tailfin regeneration. Liquid  
29 chromatography/tandem mass spectrometry reveals an increase of up to 11-fold in the  
30 number of S-nitrosylated proteins during regeneration. Among these, Kdm1a, a well-known  
31 epigenetic modifier, is S-nitrosylated on Cys334. This alters Kdm1a binding to the CoRest  
32 complex, thus impairing its H3K4 demethylase activity, which is a response specific to the  
33 endothelial compartment. Rescue experiments show S-nitrosylation is essential for tailfin  
34 regeneration, and we identify downstream endothelial targets of Kdm1a S-nitrosylation. In  
35 this work, we define S-nitrosylation as an essential post-translational modification in tissue  
36 regeneration.

37

38

39

40

41

42

43

44

45

46

47

48 **Introduction**

49 Complete regrowth of functional tissue is a highly desirable, but mostly unachieved,  
50 therapeutic target in the tissue loss associated with many human diseases. Innate immune  
51 activation is an early response to tissue stress and injury <sup>1</sup>. In lower vertebrates this is  
52 typically followed by functional tissue regeneration while in higher vertebrates there is  
53 normally fibrous scar formation <sup>2</sup>. Although several molecular pathways have been  
54 implicated in tissue regeneration, the mechanisms underlying this process are still not clearly  
55 understood <sup>3</sup>.

56 The interaction between pattern recognition receptors (PRRs) and damage-associated  
57 molecular patterns (DAMPs) during and after an injury activates molecular pathways and  
58 transcriptional factors that regulate the expression of a plethora of genes. We have previously  
59 shown that this inflammatory signaling causes global changes in the expression and post-  
60 translational modifications (PTM) of epigenetic modifiers favoring an open chromatin  
61 configuration and cellular plasticity <sup>4,5</sup>. It was also found that inducible nitric oxide synthase  
62 (iNos) translocates to the nucleus to bind and S-nitrosylate the polycomb and NuRD  
63 complexes during trans-differentiation of fibroblasts into endothelial cells <sup>6</sup>. The effect of cell  
64 autonomous innate immune signaling to increase DNA accessibility and thereby to facilitate  
65 nuclear reprogramming of cell fate is termed transflammation <sup>7</sup>. The role of this phenomenon  
66 in tissue regeneration remains unexplored.

67 Accordingly, here we investigated the role of the innate immune effector iNos and S-  
68 nitrosylation of nuclear proteins in zebrafish tailfin regeneration, an ideal model to study  
69 appendage regeneration <sup>8</sup>. We found that *inos* translocates from the cytoplasm to the nucleus  
70 in the regenerating tailfin and this is associated with an increase in S-nitrosylation of over  
71 500 different nuclear proteins. Of these, we demonstrated a strong link between Kdm1a S-

72 nitrosylation and histone demethylase activity during tailfin regeneration, specifically in  
73 endothelial cells, the main target where S-nitrosylation mostly occurs and where the S-  
74 nitrosylated form of Kdm1a promotes the expression of proangiogenic genes. Here, we show  
75 the essential role of the S-nitrosylation of nuclear proteins in tissue regeneration.

76

## 77 **Results**

78 *Nos2* translocates from the cytoplasm to the nucleus and triggers protein S-nitrosylation  
79 during tailfin regeneration.

80 Compared to mammals that have three *nos* genes (neuronal, or *nos1*; inducible, or *nos2*; and  
81 endothelial, or *nos3*), the zebrafish genome has only *nos1* and two *nos2* genes (*nos2a* and  
82 *nos2b*). Activation of the innate immune system transcription factor Nf-kb following injury  
83 triggers the translocation of the kb subunit into the nucleus which in turn promotes activation  
84 of a panoply of genes, including *inos*<sup>9</sup>. The activation of Nf-kb after tailfin amputation was  
85 measured as GFP signal in the *Tg(nfkb:EGFP)<sup>nc1</sup>* zebrafish (**Fig. S1A-B**). Real time PCR for  
86 *nos* genes measured in the adult zebrafish (*Danio rerio*) tailfin uninjured (baseline) and at 3,  
87 5 and 10 days post-amputation (dpa) revealed a significant increase of *nos2b* expression and  
88 a slight increase in *nos1* at 3 and 5 dpa (**Fig. 1A**). Increased *nos2* expression during  
89 regeneration was confirmed by western blotting (WB) (**Fig. 1B**). To confirm the role of Nf-  
90 kb on the upregulation of *nos2*, adult zebrafish were injected with the Nf-kb inhibitor Bay11-  
91 7082 30 mM, which resulted in a reduced expression of *nos2b* in the injured tailfin (**Fig.**  
92 **S1C**) at 3 and 5 dpa compared to injured control. While iNos has been considered  
93 predominantly cytosolic, it has also been localized to other cellular compartments, including  
94 the nucleus<sup>6</sup>. Analysis of *Nos2* compartmentalization in the uninjured tailfin confirmed a  
95 predominantly cytoplasmic distribution of this protein (**Fig. 1C**). However, at 3 dpa *Nos2*

96 was predominantly in the nucleus, with equal distribution between nucleus and cytoplasm at  
97 5 dpa, returning predominantly to the cytoplasm by 10 dpa, similar to uninjured controls.  
98 Thus, immediately after injury, Nos2 translocates to the nucleus and, during later stages of  
99 repair, shifts back to the cytoplasm. This key series of observations gave rise to our principal  
100 hypothesis, namely, that changes in the distribution of Nos2 during regeneration mirror and  
101 drive changes in S-nitrosylation of nuclear proteins.

102 To address this, we collected newly formed tissue at the wound edge for extraction of nuclear  
103 protein after amputation of adult zebrafish tailfins. Separation of nuclear proteins was  
104 confirmed by western blotting to detect nuclear and cytoplasmic markers (**Fig. S1D**). The  
105 nuclear fractions were treated with iodoacetyl Tandem Mass Tags (iodoTMT) to label S-  
106 nitrosylated proteins, and were subsequently identified using an anti-TMT antibody. Western  
107 blotting revealed an increase in the number and intensity of protein bands in the regenerating  
108 tissue compared to control tissue, suggesting an S-nitrosylation switch in nuclear proteins  
109 (**Fig. 1D**). When zebrafish were injected in the retro-orbital vein with increasing  
110 concentrations of the Nos inhibitor N( $\omega$ )-nitro-L-arginine methyl ester (L-NAME) or the NO  
111 scavenger 2-Phenyl-4,4,5,5-tetramethylimidazoline-1-oxyl 3-oxide (PTIO), the levels of  
112 protein S-nitrosylation were reduced (**Fig. 1E**), whereas treatment with increasing  
113 concentrations of the NO donor S-Nitroso-N-acetyl-DL-penicillamine (SNAP) increased  
114 protein S-nitrosylation (**Fig. 1E**). L-NAME and PTIO significantly reduced tailfin  
115 regeneration compared to control or SNAP treated groups at 3 and 7 dpa (**Fig. 1F and S2A**).

116 As L-NAME inhibits all Nos isoenzymes, in order to assess the specific role of iNos we  
117 treated the tailfin regeneration model with the iNos selective inhibitor 1400W<sup>10</sup>. Treatment  
118 with 1400W 50 mM reduced tailfin regeneration in a manner similar to L-NAME, suggesting  
119 that Nos2 is the main Nos isoenzyme involved in the effect observed by L-NAME (**Fig.**

120 **S2A**). Overall, these results indicate that Nos2 and NO are necessary for tailfin regeneration  
121 and that protein S-nitrosylation plays a key role in this process.

122

123 Analysis and screening of S-nitroso-proteome revealed an increase in S-nitrosylated nuclear  
124 proteins during tailfin regeneration.

125 To identify nuclear proteins that were S-nitrosylated during regeneration, we performed  
126 liquid chromatography and tandem mass-spectrometry (LC/MS/MS) (**Fig. 2A**) on protein  
127 extracts from the tailfin wound edge, excised at 3, 5 and 10 dpa. Hierarchical clustering  
128 showed a striking increase in the number of nuclear S-nitrosylated proteins during  
129 regeneration, in particular at 5 dpa (**Figs. 2B and S3**). We found that the number of nuclear  
130 S-nitrosylated proteins increased from 31 in uninjured to 199, 351 and 264 at 3, 5 and 10 dpa,  
131 respectively (**Fig. 2C**). Taking account of the fact that some proteins changed their S-  
132 nitrosylation state on more than one cysteine residue of that protein, the actual total number  
133 of S-nitrosylated peptides increased from 31 in uninjured to 332, 566 and 450 at 3, 5 and 10  
134 dpa, respectively (**Fig. S3A**). While a few proteins were S-nitrosylated throughout these time-  
135 points, suggesting constitutive S-nitrosylation, the analysis revealed that the majority of the  
136 proteins were modified uniquely at a specific time-point. These data strongly suggest a  
137 dynamic choreography of S-nitrosylation throughout the regeneration process. Indeed, an  
138 analysis of differential enrichment revealed that proteins of many different pathways are S-  
139 nitrosylated specifically during regeneration (**Fig. 2D**). Some of these are known to be  
140 implicated in developmental and wound healing processes, such as the epithelial-  
141 mesenchymal transition (EMT) pathway<sup>11</sup> and the Hedgehog pathway<sup>12</sup>. From the protein  
142 list (**Dataset S1**), we selected 31 candidates, encompassing epigenetic modifiers and  
143 transcription factors for which transient S-nitrosylation have not been previously reported and

144 that have a human ortholog (**Table S1**). We proceeded to analyse these by deep mass-  
145 spectrometry, focusing initially on Kdm1A, also known as Lsd1, Kiaa061 or Aof2  
146 (UniProtKB - F6NIA2).

147

148 S-nitrosylation of Kdm1a is associated with a reduced binding to the CoREST complex and  
149 impaired demethylase activity on H3K4 during tailfin regeneration.

150 Kdm1a was the first histone lysine-demethylase to be described<sup>13</sup>, where an amine oxidase  
151 domain mediates its FAD-dependent demethylase activity<sup>14</sup>. Kdm1a participates in gene  
152 repression as part of the CoREST (co-repressor for element-1-silencing transcription factor)<sup>15</sup>  
153 and NuRD (nucleosome remodeling and histone deacetylation)<sup>16</sup> co-repressor complexes  
154 mediating the demethylation of H3K4me1/me2. It also participates in gene activation in  
155 androgen receptor (Ar)-driven expression programs through demethylation of repressor  
156 marks H3K9me1/me2<sup>17,18</sup>. More recently, it has been demonstrated that Kdm1a is also able  
157 to demethylate lysine residues at several non-histone substrates, such as p53<sup>19</sup>, Dnmt1 (DNA  
158 (cytosine-5)-methyltransferase 1)<sup>20</sup> and E2F1<sup>21</sup>.

159 Mass-spec revealed that Kdm1a, although detectable in the nucleus at all three time-points,  
160 becomes S-nitrosylated on Cysteine 334 (Cys334) at 3 and 5 dpa (**Fig. 3A-B**). The increase  
161 of Kdm1a S-nitrosylation (S-NO) during tailfin regeneration was confirmed by western  
162 blotting for S-NO on samples previously immunoprecipitated for Kdm1a (**Fig. 3C**). Zebrafish  
163 Kdm1a protein has 85% identity with the corresponding human gene with the Cys334  
164 corresponding to Cys360 in the human ortholog (**Fig. S4A**). Intriguingly, the sequence of 60  
165 amino acids (aa) from 50 upstream to 9 downstream of the Cys334 retains 100% identity with  
166 the human ortholog. Human KDM1a crystal structure, obtained from Protein Data Bank  
167 deposited by Tan *et al.*<sup>22</sup>, is shown in **Fig. S4B**.



168 The selectivity of Kdm1a for its main targets, H3K4 and H3K9, depends on its interaction  
169 with specific protein co-factors, including CoREST, NuRD, and Ar. PTM can modulate these  
170 interactions. Therefore, first we analysed these co-factors and their complexes in injured and  
171 uninjured tailfins. Expression of CoREST and NuRD were unchanged in injured and  
172 uninjured tailfin (**Fig. S5**). The expression of *ar* was extremely low and was not different in  
173 injured versus uninjured tailfin (**Fig. S5**). Having established the patterns of expression of  
174 these co-factors, and since *ar* is associated with the modulation of H3K9, we decided to focus  
175 on H3K4 which is known to be linked to CoREST and NuRD.

176 Hence, focusing on NuRD and CoREST, we tested the hypothesis that S-nitrosylation of  
177 Cys334 affects Kdm1a binding affinity to these complexes. To do this, we performed co-  
178 immunoprecipitation with Kdm1a antibody (**Fig. 3D**), followed by WB for the members of  
179 the CoREST (Rcor1 and Hdac1) (**Fig. 3E**) and NuRD (Rbbp4 and Chd4) (**Fig. 3F**)  
180 complexes. While the binding of NuRD complex was similar during regeneration compared  
181 to control, the binding to the CoREST complex was reduced.

182 To further assess the role of Kdm1a in the adult zebrafish, knockdown (KD) was achieved by  
183 injection of morpholino (*vivo*-Mo) in the retro-orbital vein. The KD efficiency as well as  
184 delivery to the tailfin was assessed by western blotting for Kdm1a (**Fig. 4A**). We saw clear  
185 evidence that *kdm1a* KD by *vivo*-Mo injection impaired tailfin regeneration compared to  
186 controls (**Fig. 4B-C**). A dynamic and choreographed regulation of *kdm1a* expression and  
187 activity therefore appears to be essential for tissue regeneration. These data support the role  
188 of Kdm1a as a key regulator of regeneration, likely through modulation of chromatin  
189 modifications.

190 During tailfin regeneration we observed a significantly reduced demethylase activity of  
191 Kdm1a in the regenerating tailfin associated with increased levels of Kdm1a S-nitrosylation

192 **(Fig. 3B)**. This reduced Kdm1a activity was similar to that observed in zebrafish *kdm1a* KD  
193 **(Fig. S6)**.

194 Indeed, at the same time that Kdm1a activity was reduced, there was a corresponding  
195 reduction in unmethylated H3K4 **(Fig. 4D-E)**. By contrast, there was an increase in  
196 H3K4me1/me2, normally associated with active gene transcription **(Fig. 4D-E)**. H3K4me3  
197 showed a pattern similar to H3K4me2. However, it is known that Kdm1a is unable to  
198 demethylate H3K4me3, according to the chemical nature of the amine oxidation reaction  
199 catalyzed by flavin-containing amine oxidases, thus precluding H3K4me3 as a substrate<sup>13</sup>.

200 In regenerating tailfins, the blastema, a pool of proliferative progenitor cells, is located at the  
201 distal region of the tailfin while cells in the proximal region undergo differentiation. To  
202 localise the region in which Kdm1a S-nitrosylation is most important, we analysed the  
203 expression of *kdm1a* gene in the distal (blastema) and proximal regions (differentiating zone)  
204 of regenerating tailfins at 3 and 5 dpa. Compared to uninjured tailfins, *kdm1a* expression was  
205 significantly lower in the blastema and only slightly reduced in the proximal differentiating  
206 zone **(Fig. S7A)**. We also took advantage of a publicly available single cell(sc) RNA-seq  
207 dataset obtained in the regenerating tailfin<sup>23</sup> in which *kdm1a* expression was detected, at low  
208 levels, with a distinct expression pattern observed in specific cell types **(Fig. S7B)**. For  
209 example, compared to preinjury, the *kdm1a* expression was reduced in mucosal-like cells at 1  
210 and 2 dpa followed by an increase at 4 dpa, it was increased in mesenchymal cells and it was  
211 not expressed in hematopoietic cells during the regeneration. Overall, this data provides  
212 further evidence that modulation of S-nitrosylation, as well as modulation of gene expression,  
213 is a key mechanism regulating the functionality of Kdm1a during tailfin regeneration.

214

215 *Kdm1a* is S-nitrosylated preferentially in the endothelial cells of the regenerating tailfin.

216 Next, we identified S-nitrosylation associated with specific cell type. The formation of new  
217 blood vessels is a crucial process during wound healing and tissue repair, similar to  
218 embryogenesis and early growth. During tailfin regeneration, endothelial cells within the  
219 growing blood vessels sprout and invade adjacent avascular areas. By using the  
220 *Tg(fli1:EGFP)<sup>y1</sup>* zebrafish line, where endothelial cells (EC) fluoresce green (GFP<sup>+</sup> cells), we  
221 detected the formation of new blood vessels in the regenerating tailfin at 2 dpa that become a  
222 dense vascular plexus by 3 dpa (**Fig. 5A**) consistent with previous observations<sup>24</sup>. We  
223 isolated EC from these tailfins and performed FACS analysis. We found an increase in the  
224 percentage of EC (GFP<sup>+</sup>) from  $4.3 \pm 0.3$  % to  $6.1 \pm 0.4$  %, in the uninjured versus injured  
225 tailfin, respectively (**Fig. 5B-C and S7C**). We FACS purified GFP<sup>+</sup> (EC) and GFP<sup>-</sup> (non-EC)  
226 from injured and uninjured tailfins, extracted RNA and performed real time PCR. For *kdm1a*,  
227 we found no difference in gene expression between groups (**Fig. S8A**). We also analysed the  
228 expression of CoREST (*rcor1* and *hdac1*) and NuRD (*rbbp4* and *chd4*) factors and did not  
229 detect significant differences between groups (**Fig. S8B-E**). In response to stress or injury,  
230 EC upregulate *inos*, with consequent NO production<sup>25</sup>. We found an upregulation of *nos2b*  
231 compared to *nos2a* and *nos1* genes in the EC of injured tailfins compared to uninjured (**Fig.**  
232 **S8F-H**). Therefore, we investigated if S-nitrosylation, more specifically of Kdm1a, occurs in  
233 EC during tailfin regeneration. We observed an overall increase in S-nitrosylated proteins in  
234 the EC of regenerating tissue compared to EC from uninjured tissue (**Fig. 5D**), with no  
235 change in S-nitrosylated proteins in GFP<sup>-</sup> cells from injured versus uninjured tailfins. Then,  
236 we specifically analysed S-nitrosylated Kdm1a in EC cells from injured and uninjured tailfins  
237 at 5 dpa, including an injured group treated with the nitric oxide (NO) scavenger PTIO.  
238 While the expression of total *kdm1a* did not change in the three groups, S-nitrosylated  
239 Kdm1a was detectable in EC from regenerating tailfin only (**Fig. 5E**), while it was abolished

240 in the group treated with PTIO. The increased S-nitrosylation of Kdm1a in EC of the  
241 regenerating tailfin was associated with a significant increase in vessel density compared to  
242 the other two groups (**Fig. 5F**).

243

244 S-nitrosylation of Kdm1a is associated with increased H3K4me2 marks for endothelial genes  
245 during tailfin regeneration.

246 As shown in **Fig. 4D-E**, H3K4me2, a target of Kdm1a, is increased during regeneration  
247 associated with the reduced demethylase activity of the S-nitrosylated form of Kdm1a.  
248 Methylated H3K4 is associated with active gene transcription. Accordingly, we reasoned that  
249 an increased occupancy of H3K4me2 would result in increased levels of proangiogenic  
250 factors. To address this hypothesis, and investigate whether the increased vessel density  
251 observed during regeneration was correlated to S-nitrosylation of Kdm1a, we performed  
252 Chromatin Immunoprecipitation using a ChIP-grade antibody specific for H3K4me2,  
253 followed by PCR for 10 well-known proangiogenic factors, including *kdr*, *vegfaa*, *fgf2*,  
254 *angpt2*, *tek*, *tie1*, *cdh5*, *cd31*, *mmp2* and *tbx20*. ChIP-PCR showed that the occupancy of  
255 H3K4me2 on *vegfaa* and *tek* in endothelial cells from injured tailfins was significantly higher  
256 compared to injured tailfins treated with PTIO and higher than uninjured tailfins (**Fig. 5G**).  
257 Furthermore, real time PCR showed that expression of 7 out of 10 proangiogenic factors,  
258 including *vegfaa* and *tek*, were significantly increased during regeneration (**Fig. 5H**), whereas  
259 they were unchanged following treatment with PTIO, again suggesting that nitric oxide was  
260 driving or facilitating angiogenesis via a mechanism involving S-nitrosylation.  
261 Overall, these findings show that endothelial cells of the regenerating tissue are a key cell  
262 target for protein S-nitrosylation after injury and that Kdm1a is specifically S-nitrosylated in  
263 these cells. S-nitrosylation of Kdm1a reduces Kdm1a demethylase activity and, as a

264 consequence, more H3K4me2 will accumulate in the genome. In particular, we found  
265 increased occupancy of H3K4me2 on *vegfaa* and *tek*.

266 This does not exclude, however, that other S-nitrosylated proteins among those arising from  
267 the mass-spec dataset could be implicated in endothelial cells and vascular regrowth as well  
268 as in other cell types.

269 Next, to investigate the effects of the absence of the Kdm1a C334 S-nitrosylation site on  
270 tailfin regeneration we synthesized, by site-directed mutagenesis, a mutant variant of Kdm1a  
271 mRNA where the cysteine 334 was substituted with alanine (C334A), that cannot be S-  
272 nitrosylated (**Fig. 6A**). These experiments assessed the ability of this mutated Kdm1a mRNA  
273 to rescue the morpholino (Mo) phenotype compared to wild-type mRNA. However, contrary  
274 to the MO oligo that is a stable molecule, not degraded by the nucleases, the mRNA is prone  
275 to degradation by nucleases, well before reaching the tailfin, *i.e.* the tissue under study.  
276 Therefore, we decided to perform these studies in the zebrafish embryos where the  
277 cytoplasmic bridges connecting the early embryonic cells allow rapid diffusion of mRNA  
278 into the cells, resulting in fast and ubiquitous delivery<sup>26</sup>.

279 Before the morpholino (Mo) studies, real time PCR analysis confirmed *kdm1a* expression  
280 during development, with a slight reduction from 24 to 120 hpf (**Fig. S9A**). This finding was  
281 also useful to optimise the dose of Mo to inject. Mo experiments were conducted according  
282 to the guidelines<sup>2627</sup> using several controls to assess morpholino specificity for *kdm1a*. First,  
283 we injected *kdm1a*-targeted Mo or the mismatch (control), using an optimized dose of 0.8 ng  
284 per egg. The effective *kdm1a* KD was confirmed by western blotting (**Fig. 6B**). The survival  
285 rate of *kdm1a* KD embryos at 120 hpf was approximately 80 % compared to 90 % in controls  
286 (**Fig. S9C**). *Kdm1a* KD embryos did not show gross abnormalities compared to control (**Fig.**  
287 **S9D**), however we found reduced blood flow velocity (**Fig. S9E**) and reduced expression of

288 *gatal* (**Fig. S9F**), a red blood cell marker, consistent with a previous report<sup>28</sup>. To confirm  
289 these effects and to exclude sequence-specific off-target effects we used a second Mo with  
290 non-overlapping sequence to compare phenotypes with the first Mo. Indeed, both Mo  
291 injections induced *kdm1a* knockdown and produced a comparable phenotype. To further  
292 confirm the specificity, we co-injected half-doses of each Mo, such that the phenotype was  
293 only just apparent with each Mo alone, but with clear additive effects on phenotype when co-  
294 injected. Specifically, the two *kdm1a* -targeted antisense Mo were co-injected each at 1/2  
295 dose (0.4 ng per egg). While the phenotype was apparently unaffected with 1/2 dose of each  
296 oligo injected alone, the co-injection of half doses together produced phenotypic effects  
297 similar to those produced by a single oligo at full dose (0.8 ng per egg) (**Figs. 6B and S9**).  
298 These additive effects of low doses of two antisense oligos strongly supports a *kdm1a* -  
299 specific effect. We did not find an increase in expression of *tp53*, well-known off-target  
300 effect, at the dose of Mo used in this study, therefore we did not co-inject *tp53*-Mo for *tp53*  
301 gene silencing (**Fig. S9B**). We observed that the regeneration of the tailfin was significantly  
302 reduced in *kdm1a* KD embryos compared to control (**Fig. 6C-D**), with a phenotype  
303 penetrance of >70%. The phenotype of *kdm1a* morphants was rescued by co-injecting *kdm1a*  
304 mRNA indicating that the observed effects were specific for *kdm1a*. This also clearly shows a  
305 key role of *kdm1a* in tailfin regeneration. However, *kdm1a* mRNA C334A did not rescue  
306 tailfin regeneration (**Fig. 6C-D and Fig. S9**). This further confirmed the crucial role of S-  
307 nitrosylation of this specific cysteine residue on Kdm1a in modulating tailfin regeneration.

308

## 309 **Discussion**

310 Following stress or injury, *inos* is activated within local somatic cells<sup>29</sup>, leading to protein S-  
311 nitrosylation, the covalent attachment of a NO group to the thiol side chain of the cysteine.

312 This mechanism has emerged as a dynamic, post-translational regulatory mechanism for  
313 many classes of proteins<sup>30</sup>. We found increased expression of *inos* in the nuclei of the  
314 regenerating tailfin of the zebrafish, and over 500 nuclear proteins that became S-nitrosylated  
315 during regeneration. Of these, we identified a key role for Kdm1a. We demonstrated a strong  
316 link between Kdm1a S-nitrosylation and its role in histone demethylation and ultimately in  
317 regeneration of the zebrafish tailfin. Endothelial cells, where *inos* expression increases after  
318 stress or injury, seems to be the main cell target where S-nitrosylation, including of Kdm1a,  
319 mostly occurs. The essential role of Kdm1a in hematopoiesis has been shown in vitro<sup>31,32</sup> and  
320 in vivo<sup>33,34</sup>. As such, understanding the molecular mechanisms underpinning the action of  
321 Kdm1a are currently being investigated to find specific inhibitors that could be harnessed as a  
322 therapeutic strategy in cancer<sup>35</sup>. According to our bioinformatic analysis of single cell-  
323 RNAseq, *kdm1a* was not detected in hematopoietic cells of the zebrafish regenerating tailfin.  
324 Nonetheless, given the role of the Kdm1a in hematopoiesis we cannot exclude the possibility  
325 that impaired fin regeneration in *kdm1a* knockdown zebrafish could, at least partially, derive  
326 from systemic effects associated with altered immune cell function.

327 In our study, the S-nitrosylated form of Kdm1a has a reduced demethylase activity on H3K4  
328 that results in a corresponding increase in H3K4me2 that, by turn, promotes the expression of  
329 proangiogenic genes. This is the first study to show the importance of the S-nitrosylation of  
330 nuclear proteins in tissue regeneration and potentially opens up new therapeutic avenues (**Fig.**  
331 **6E**).

332 While many interesting candidate S-nitrosylated nuclear proteins were identified (**Dataset S1**  
333 **and Table S1**), we focused on Kdm1a. However, we predict that it is likely that Kdm1a is  
334 not the only rate limiting factor. It is likely that modulating the expression and S-nitrosylation  
335 of other candidates could result in similar effects on regeneration, possibly by acting via the  
336 same cells and pathways identified here but possibly on other cell types and pathways. This

337 would depend on the effects that S-nitrosylation has on molecular networking of each protein  
338 candidate. For example, S-nitrosylation of Hexim1 (hexamethylene bisacetamide inducible  
339 protein 1) could affect its binding in the P-TEFB complex<sup>36</sup> and potentially inhibits the Cdk9  
340 kinase activity and the transcription of genes specific to regeneration.  
341 Aberrant levels of protein S-nitrosylation have been implicated in a number of diseases,  
342 including heart disease, diabetes, cancer, neurological disorders, chronic degenerative  
343 diseases, and inflammatory disorders (reviewed in<sup>37</sup>), regeneration. Furthermore, very little  
344 is known about two important aspects of this process, firstly the extent and the dynamics of  
345 S-nitrosylation of *nuclear* proteins in human disease and secondly the role of S-nitrosylation  
346 of nuclear proteins during tissue repair and regeneration<sup>38</sup>. Our paper is the first to examine  
347 the mechanisms and potential role of S-nitrosylation of nuclear proteins during tissue  
348 regeneration in vivo and provides several important observations that implicate S-  
349 nitrosylation of nuclear proteins in regeneration.

## 350 **Methods**

### 351 Ethical approval

352 This work complied with all relevant ethical regulations for animal testing and research.  
353 Animals were housed and all experiments were carried out in accordance with the  
354 recommendations of the Institutional Animal Care and Use Committee at the Houston  
355 Methodist Research Institute, and with the United Kingdom Animals (Scientific Procedures)  
356 Act 1986 at the Queens Medical Research Institute research facilities.

357

### 358 Zebrafish aquaculture and husbandry

359 Adult zebrafish – wild-type *Wik* and *Tg(nfkb:EGFP)<sup>nc1</sup>* strains – were maintained according  
360 to standard procedures. Fish were kept at 28°C under a 14/10 h light/dark cycle and fed with



361 dry meal (Gemma Micro, Westbrook, ME) twice per day. Embryos were obtained by natural  
362 mating and kept in E3 embryo medium at 28.5°C. Surgical procedures were performed under  
363 anaesthesia with Tricaine (also named MS-222, Sigma-Aldrich, St Louis, MO, cat. E10521)  
364 0.02 mg/ml on embryos and 0.05 mg/mL in adult zebrafish.

365

#### 366 Zebrafish tailfin amputation and regeneration

367 Caudal tailfin amputation surgeries were performed as previously described<sup>39</sup>. Briefly, fish  
368 were anaesthetized and amputations were made by using a sterile razor blade, removing half  
369 of the tailfin. At day 3, 5 and 10 post-amputation (dpa) (uninjured tailfin was used as control)  
370 the regrown tissue was carefully resected and immediately processed for nuclear protein  
371 extraction. Total regeneration was measured as previously described<sup>40</sup>. Briefly, fin images  
372 were collected before amputation and time points after amputation. The new tissue area (in  
373 pixels) of the caudal fin from the new distal fin edge to the amputation plane was quantified  
374 in each fish using Image J software. The percentage of regeneration for each fin at each time  
375 point was defined as percentage of regeneration = 100 x (regenerated tissue area/original fin  
376 area amputated). The collection of the distal (blastema) and proximal (regenerating) regions  
377 of the tailfin tissue for PCR analysis was performed under a fluorescence stereomicroscope  
378 Leica M205. The *Tg(fli1:EGFP)* zebrafish was used and the distal ends of the newly forming  
379 (GFP<sup>+</sup>) vessel branches was used as boundary to separate by dissection the two regions.  
380 Then, we placed the tissues in an Eppendorf tube and immediately extracted RNA that was  
381 used for PCR analysis.

382

#### 383 Blood vessel density

384 At 5 dpa, the adult *Tg(fli1:EGFP)* zebrafish were anesthetized. Then, fish were transferred on  
385 a wet sponge, previously soaked in tank water, to keep the zebrafish skin moist during  
386 imaging. Images of the caudal fin including the regenerated tissue were captured under a  
387 fluorescence stereomicroscope Leica M205 equipped with a camera. The images were  
388 collected with a Leica LAS X software and analysed by Image J software. The second and  
389 third rays from the dorsal edge of the fin were used for measurement of vessel area and  
390 reported as mm<sup>2</sup>.

391

## 392 Protein Extraction

393 *Extraction of nuclear proteins* - Nuclear proteins were extracted from the caudal fin tissue  
394 using the NE-PER Extraction Reagents kit (Thermo Fisher Scientific, San Jose, CA, cat.  
395 78833) according to the manufacturer's instructions, supplemented with protease inhibitor  
396 cocktail. In brief, regenerating tailfin tissue was resected, cut into small pieces and placed in  
397 a microcentrifuge tube. Then, tissue was washed three times with chilled PBS, centrifuged at  
398 500g for 1 min and supernatant discarded. Using a motor-driven pestle (Sigma-Aldrich, St  
399 Louis, MO, cat. Z359971), tissue was homogenized in solution CER I, that breaks plasma  
400 membrane but not nuclei, added with protease/phosphatase inhibitors cocktail (1:100,  
401 Thermo Fisher Scientific, San Jose, CA, cat. 78442). The tube was vigorously vortexed for  
402 30 s and put on ice for 10 min. Then, chilled CER II was added to the tube, vortexed for 10 s  
403 and incubated on ice for 1 min. The tube was centrifuged for 5 min at 16,000g and the  
404 supernatant, containing cytoplasmic proteins, was transferred to a clean pre-chilled tube and  
405 stored at -80 °C. The pellet, containing nuclei, was resuspended in chilled NER solution,  
406 vortexed on the highest setting for 15 s. The sample was placed on ice for 45 min, vortexed

407 for 20 s every 10 min. Then, the tube was centrifuged at 16,000g for 10 min and the  
408 supernatant, containing nuclear extract, immediately transferred to a clean pre-chilled tube.  
409 *Extraction of total proteins* - Zebrafish embryos were euthanised with an overdose of  
410 tricaine, washed three times in PBS and homogenized with a motor-driven pestle (Sigma-  
411 Aldrich, St Louis, MO, cat. Z359971) in 100 mL RIPA buffer (25 mmol/L Tris-HCl pH 7.6,  
412 150 mmol/L NaCl, 1% NP-40, 1% sodium deoxycholate, 0.1% SDS), supplemented with  
413 protease/phosphatase inhibitors. The lysate was kept on ice for 40 min. Then, the tube was  
414 centrifuged at 3000g for 5 min and the supernatant transferred to a clean pre-chilled tube.  
415 In both nuclear and total proteins extraction, bicinchoninic acid (BCA) protein assay (Thermo  
416 Fisher Scientific, San Jose, CA, cat. 23225) was used to measure protein concentration.

417

#### 418 Labelling of protein S-nitrosothiols

419 Labelling of S-nitrosothiols in nuclear proteins was achieved using Iodoacetyl Tandem Mass  
420 Tag (iodoTMT) kit (Thermo Fisher Scientific, San Jose, CA, cat. 90103). First, nuclear  
421 protein extracts were acetone-precipitated at -20°C for 2 h, then centrifuged at 15000g for 10  
422 min and the pellet solubilized in 500 mL HENS buffer (Thermo Fisher Scientific, San Jose,  
423 CA, cat. 90106) at a protein concentration of 1 mg/ml. Equal amounts of nuclear protein from  
424 each sample were iodoTMT-labelled. To generate a positive control sample, an aliquot of  
425 protein from control was added with 200µM S-nitrosoglutathione (GSNO, Sigma-Aldrich, St  
426 Louis, MO, cat. N4148) for 30 min at room temperature (RT). Experimental samples were  
427 incubated for 30 min at RT after adding MMTS (10µL of 1 M) to block free cysteine thiols.  
428 Then, proteins were precipitated with pre-chilled acetone (1 ml per sample) at -20°C for 2 h  
429 to remove MMTS. Samples were centrifuged at 10,000g for 10 min at 4°C, the pellet  
430 resuspended in 500 ml of HENS buffer and to each was added 5 ml of iodoTMT reagent,

431 previously dissolved in liquid chromatography/mass spectrometry (LC/MS)-grade methanol,  
432 and 10 $\mu$ L of 1M sodium ascorbate (Sigma-Aldrich, St Louis, MO, cat. A4034). As a negative  
433 control, 10 $\mu$ L of ultrapure water instead of sodium ascorbate was added in a protein sample.  
434 All samples were incubated for 1 h at 37°C, protected from light. The reaction was quenched  
435 by adding 20  $\mu$ L of 0.5M DTT and incubated for 15 min at 37°C, protected from light. All  
436 experimental samples labelled with iodoTMT sixplex were combined, added with six  
437 volumes of pre-chilled acetone and incubated at -20°C overnight. The sample was  
438 centrifuged at 10,000g for 10 min at 4°C and the pellet dissolved in 3 ml HENS buffer. Then,  
439 100 $\mu$ L of 0.5 M iodoacetamide were added and the sample incubated at 37°C for 1 h  
440 protected from light. Sample was precipitated with pre-chilled acetone and the pellet allowed  
441 to dry for 10 min.

442

#### 443 Protein digestion for mass-spec analysis

444 The pellet was dissolved in 50mM ammonium bicarbonate (Sigma-Aldrich, St Louis, MO,  
445 cat. 09830) and digested using trypsin enzyme (GenDepot, cat. T9600) at 37°C overnight.

446 The peptide mixture was acidified using 10% formic acid and dried using a vacuum  
447 concentrator (Thermo Fisher Scientific, San Jose, CA, cat. SPD120).

448

#### 449 Enrichment of iodoTMT-labeled S-nitrosopeptides

450 The anti-TMT Antibody Resin (Thermo Fisher Scientific, San Jose, CA, cat. 90076) was  
451 washed three times with Tris Buffered Saline (TBS) (Thermo Fisher Scientific, San Jose, CA,  
452 cat. 28358). Previous labeled and lyophilized peptides were resuspended in TBS (a small  
453 portion of unfractionated sample was stored for direct analysis of the non-enriched samples).  
454 Then, peptides were added to the anti-TMT resin (100 $\mu$ L of settled resin for every 1 mg of

455 iodoTMT Reagent-labeled peptides) and incubated at RT for 4 h. Finally, the resin was  
456 washed three times (5 min per wash) with TBS and then three times with water. The sample  
457 was eluted with TMT Elution Buffer (Thermo Fisher Scientific, San Jose, CA, cat. 90104).  
458 The eluate was frozen and lyophilized, using a vacuum concentrator and then the sample  
459 resuspended in a solution of 5% methanol/0.1% formic acid. Then, 1-5 $\mu$ L of sample were  
460 injected directly onto an LC-MS/MS system.

461

#### 462 LC/MS-MS

463 The mass spectrometry analysis of S-nitrosopeptides was carried out on a nano-LC 1200  
464 system (Thermo Fisher Scientific, San Jose, CA) coupled to Orbitrap Fusion™ Lumos ETD  
465 (Thermo Fisher Scientific, San Jose, CA) mass spectrometer. The peptides were loaded onto  
466 a Reprosil-Pur Basic C18 (1.9  $\mu$ m, Dr. Maisch GmbH, Germany) pre-column of 2 cm X 100  
467  $\mu$ m and in-lined an in-housed 5 cm x 150  $\mu$ m analytical column packed with Reprosil-Pur  
468 Basic C18 beads. The peptides were separated using a 75 min discontinuous gradient of 5-  
469 28% acetonitrile/0.1% formic acid at a flow rate of 750nl/min. The eluted peptides were  
470 directly electro-sprayed into the mass spectrometer. The instrument used the multi-notch  
471 MS3-based TMT method. The full MS scan was performed in Orbitrap in the range of 375-  
472 1500m/z at 120000 resolution followed by ion trap CID-MS2 fragmentation at precursor  
473 isolation width of 0.7 m/z, AGC of 1X104, maximum ion accumulation time of 50ms. The  
474 top ten fragment ions from MS2 was selected for HCD-MS3 with isolation width of 2 m/z,  
475 AGC 5X104, collision energy 65%, maximum injection time of 54ms. The RAW file from  
476 mass spectrometer was processed with Proteome Discoverer 2.1 (Thermo Fisher Scientific,  
477 San Jose, CA) using Mascot 2.4 (Matrix Science) with percolator against Zebrafish Uniprot  
478 database. The precursor ion tolerance and product ion tolerance were set to 20 ppm and

479 0.5Da respectively. Variable modifications of oxidation on Methionine (+15.995Da) and  
480 iodoTMT tag (+329.2266Da) on cysteine residues was used. The general quantification in  
481 consensus workflow used unique and razor peptides with top 3 peptides for area calculation,  
482 while reporter quantification used co-isolation threshold of 50 and average reporter S/N  
483 threshold of 10. The assigned peptides and PSMs were filtered at 1% FDR.

484

#### 485 Bioinformatic analysis

486 The computational detection strategy identifies peptides exhibiting iodoTMT tag  
487 modifications. Proteome Discoverer software (Thermo Fisher Scientific, San Jose, CA) was  
488 used to search MS/MS spectra against the Zebrafish UniProt database (Danio rerio;  
489 UP000000437) using Mascot 2.3 search engine. The iodoTMTsixplex quantification method  
490 within Proteome Discoverer software was used to calculate the reporter ratios with a mass  
491 tolerance  $\pm 10$  ppm. Search algorithms, including MS-Fragger was also used in the analysis.  
492 Hierarchical clustering of S-nitrosylated protein expression heatmap was conducted using  
493 MEV based on Pearson correlation distance metric and the average linkage method.  
494 Ingenuity pathway analysis (IPA, Ingenuity systems Qiagen, Redwood City, CA) was used to  
495 assess Gene Ontology (GO) and IPA analysis to explore the function of differential S-  
496 nitrosylated proteins. Enrichment Q values of S-nitrosylated protein pathways were defined  
497 based on EdgeR FDR cutoff  $1e-5$ . The GO category was classified by Fisher's exact test, and  
498 the p-value was corrected by the false discovery rate (FDR) calculation.

499 The scRNA-seq of the regenerative caudal fin was analysed following the methods described  
500 in the manuscript<sup>23</sup>. The matrix count from cell ranger were obtained on GEO database  
501 accession GSE137971. Downstream analysis was performed on R using the package Seurat.  
502 Clustering analysis was performed on the integrated dataset and we found 6 clusters. These

503 clusters were annotated as Superficial/intermediate/basal epithelial, mucosal-like,  
504 hematopoietic and mesenchymal based on markers described in Hou et al.<sup>23</sup>. Differential  
505 gene expression between the different time points compared to pre-injury was done using the  
506 function FindMarkers from Seurat (based on Wilcoxon test followed by Bonferroni  
507 correction). Violin Plot of *kdm1a* expression was obtained using the Vln Plot function of  
508 Seurat.

509

510 Chromatin immunoprecipitation (ChIP)-PCR assay  
511 ChIP assay was performed following the manufacturer's instructions (Cell Signalling  
512 Technology, Beverly, MA). Briefly, 15 tailfins of adult zebrafish per group were  
513 disaggregated in single cells as described above. DNA and protein were crosslinked by 1%  
514 formaldehyde. Chromatin was isolated and digested with Micrococcal Nuclease. Then, the  
515 DNA-protein complex was precipitated with control IgG or antibody against H3K4me2  
516 (rabbit polyclonal, ChIP grade) overnight at 4°C and protein A/G conjugated magnetic beads  
517 for 1 hr. Cross-links were reversed. The extracted DNA was used as template for PCR  
518 amplification of the targeted promoter region. The extracted DNA from unprecipitated DNA-  
519 protein complex was used as input. The promoter regions of 10 genes known to be involved  
520 in neoangiogenesis (*kdr*, *vegfaa*, *cdh5*, *tek*, *tie2*, *tbx20*, *fgf2*, *angpt2*, *mmp2*, *cd31*) were  
521 identified in ENSEMBL. The gene sequence up to 600 bp upstream of the TSS was validated  
522 this sequence on genome.ucsc.edu to confirm it was upstream of our gene of interest. We also  
523 looked for the presence of CpG islands and TATA box. Hence, we designed four couples of  
524 primers using Primer Blast for each gene that matched in this region and around the TSS, and  
525 that could generate amplicons which size was no more than 120-130 bp to allow both primers  
526 to find their target on one fragment of ChIP DNA, if present. In-silico PCR (UCSC) was used

527 to confirm that primers matched our region of interest and the amplicon size, and then  
528 primers were further validated by PCR using genomic DNA.

529

### 530 Quantification of Kdm1a demethylase activity

531 Kdm1 Activity Colorimetric Kit (Abcam, Cambridge, UK, cat. ab113459) was used to  
532 quantify Kdm1 activity. Nuclear proteins were extracted from the regenerating caudal fin as  
533 shown above and an input of 10µg per sample was used for the enzymatic analysis. The  
534 experiment was run in triplicate. A standard curve was prepared with Kdm1a assay buffer  
535 and assay standard solution, containing demethylated histone H3K4, diluted at concentration  
536 between 0.2 and 5 ng/µl. Sample wells were added with Kdm1a assay buffer, Kdm1a  
537 substrate (containing di-methylated histone H3K4) and 10µg of nuclear extract. No nuclear  
538 extract was added in blank wells. The strip-well microplate was covered with adhesive film  
539 to avoid evaporation, and incubate at 37°C for 2 h. At this stage, active Kdm1a binds to the  
540 substrate and removes methyl groups from the substrate. Then, the reaction solution was  
541 removed and each well washed three times with wash buffer. Capture antibody, that  
542 recognizes Kdm1a-demethylated products, was added to each well, the strip-well was  
543 covered with aluminum foil to protect from light and incubated at RT for 60 min. Antibody  
544 solution was removed and each well washed three times with wash buffer. Then, detection  
545 antibody was added to each well, covered again with aluminum foil and incubated at RT for  
546 30 min. Detection antibody solution was removed and each well was washed four times with  
547 wash buffer. Developer solution was added and the microplate incubated at RT for 10 min  
548 protected from light. In presence of methylated DNA, the solution will turn blue. At this  
549 point, stop solution was added to each well to quench the enzymatic reaction. Absorbance  
550 was read on a microplate reader Infinite M1000 (Tecan, Männedorf, Switzerland) at a



551 wavelength at 450 nm with an optional reference wavelength of 655 nm. The activity of  
552 Kdm1a enzyme is proportional to the optical density (OD) intensity measured. Accordingly,  
553 Kdm1a activity was calculated using the following formula:  
554 
$$\text{Kdm1a activity (OD/min/mg)} = \frac{\text{Sample OD} - \text{Blank OD}}{\text{Protein Amount } (\mu\text{g}) \times \text{min}}.$$

555

#### 556 *Kdm1a* suppression

557 The knockdown (KD) of *kdm1a* gene (NM\_001242995.1) in zebrafish was achieved by  
558 injection of antisense morpholino (Mo) (Gene Tools, Philomath, Oregon) oligo targeting the  
559 mRNA AUG translational start site (sequence 5'-TTGGACAACATCACAGATGACAGAG-  
560 3'). A 5-base pair mismatch Mo (sequence 5'-TTGcAgAACATgACAcATcACAGAG-3')  
561 was used as control to detect possible off-target effects. A second antisense oligo targeting  
562 i3e4 splice junction of *kdm1a*, sequence 5'-CTACACCTGAGAAACCCAACATTTTC-3' was  
563 used to corroborate data obtained with MOs that block translation.

564 Using a standard microinjector (IM300 Microinjector; Narishige, Tokyo, Japan), an  
565 optimized dose of 0.4 ng (0.5nL bolus) of morpholino placed in a pulled glass capillary was  
566 injected in each embryo at 1–2 cell stage, just beneath the blastoderm.

567 For KD of *kdm1a* in adult zebrafish, a vivo-Mo version was used, where the standard Mo is  
568 bound to a synthetic scaffold containing guanidinium groups as a delivery moiety in adult  
569 tissues. An antisense vivo-Mo that targets human b-globin intron mutation 5'-

570 CCTCTTACCTCATTACAATTTATA-3' was used as negative control (Gene Tools LLC,  
571 Philomath, Oregon). Adult zebrafish were anesthetized in tricaine 0.05 mg/mL, and 2  $\mu$ L of  
572 0.1 mmol/L vivo-Mo solution, previously loaded in a glass capillary, was injected into the  
573 retro-orbital vein, as previously described<sup>41</sup>, on days 10, 8, 6, 4, 2 and 0 before tailfin  
574 amputation.

575 *kdm1a* construct

576 A construct with *kdm1a* gene of *Danio rerio* (NM\_001242995.1) was prepared to generate  
577 *kdm1a* modified (m) mRNA and was assembled from synthetic oligonucleotides.  
578 Modifications in the triplet code (n=7 silent mutations) were inserted in the sequence  
579 corresponding to the mRNA AUG translational start site (*i.e.* Mo binding site) to prevent Mo  
580 recognition in rescue experiments. The fragment was inserted in the pMA (GeneArt,  
581 Invitrogen, Carlsbad, CA) cloning vector and cloned in transformed *Escherichia coli* bacteria  
582 (strain K12/DH10B, Invitrogen, Carlsbad, CA) and then purified. The final construct was  
583 verified by sequencing and the sequence identity within the insertion site was 100%.

584

585 Site-Directed Mutagenesis

586 Site-directed mutagenesis of *Kdm1a* was carried out with Q5 Site-Directed Mutagenesis kit  
587 (New England Biolabs, Ipswich, MA, cat. E0554) according to manufacturers' instructions.  
588 Standard primers for *kdm1a* were used for exponential amplification of the plasmid DNA (F  
589 5'-GACAGCCAGTCGAGGAGAAC-3' and R 5'-TGCGACGTACGAGTATGAGC-3'),  
590 and mutagenic primers to create substitution of Cys334-to-Ala (C334A) in the plasmid were  
591 designed with the software NEBase Changer (F 5'-AAAACAGAAGGCTCCCCTCTATGA  
592 GGC-3' and R 5'-ATCTTAGCCAGCTCCATATTG-3').

593

594 In vitro transcription of *kdm1a*

595 Wild type and mutated *kdm1a* mRNA (C334A), with 7-methyl guanosine cap structure at the  
596 5' end and poly(A) tail at the 3' end, was transcribed from the constructs using HiScribe T7  
597 ARCA mRNA Kit (New England Biolabs, Ipswich, MA, cat. E2060) following  
598 manufacturers' instructions.

599 Rescue of *kdm1a* knockdown by Kdm1a mRNA

600 To determine whether the effects of the *kdm1a* KD on zebrafish embryos phenotype and  
601 tailfin regeneration were specifically due to loss of *kdm1a*, we co-injected *kdm1a* -Mo with  
602 *kdm1a* mRNA wild-type as a rescue. A bolus of 1 nl of solution containing 0.5 ng of *kdm1a*-  
603 Mo a and 1 ng of Kdm1a RNA wild-type was injected into each egg.

604

605 Rescue of *kdm1a* knockdown by *kdm1a* mRNA C334A

606 Co-injection of *kdm1a* -Mo and *kdm1a* mRNA C334A was performed to assess whether the  
607 absence of the S-nitrosylated cysteine affected the ability of the mRNA to rescue phenotype  
608 and tailfin regeneration associated with *kdm1a* KD. A bolus of 1 nl of solution containing 0.5  
609 ng of *kdm1a* -Mo and 1 ng of *kdm1a* mRNA C334A was injected into each egg.

610

611 Pharmacological modulation of S-nitrosylation

612 Adult zebrafish were anesthetized in tricaine 0.05 mg/mL. A solution of 2  $\mu$ L of iNos  
613 inhibitor N( $\omega$ )-nitro-L-arginine methyl ester (L-NAME, Sigma-Aldrich, St Louis, MO, cat.  
614 N5751) 10 or 50 mM diluted in sterile PBS (from stock solution of 250 mM), or of nitric  
615 oxide (NO) scavenger Phenyl-4,4,5,5-tetramethyl imidazoline-1-oxyl 3-oxide (PTIO, Sigma-  
616 Aldrich, St Louis, MO, cat. P5084) 3 or 10 mM diluted in sterile PBS (from stock solution of  
617 100 mM), or of NO donor S-Nitroso-N-acetyl-DL-penicillamine (SNAP, Sigma-Aldrich, St  
618 Louis, MO, cat. N3398) 10 or 30 mM diluted in DMSO (from stock solution of 100 mM), or  
619 PBS as control, was loaded on a glass capillary, prepared in advance with a micropipette  
620 puller (Narishige, Inc., PC-10) and connected to a microinjector (IM300 Microinjector;

621 Narishige, Tokyo, Japan) and was injected into the retro-orbital vein as previously described  
622 <sup>41</sup> on days 6, 4, 2 and 0 before tailfin amputation.

623 The concentration of the Nos inhibitors, L-NAME and 1400W, were adopted after a pilot  
624 study with doses up to 250 mM. The survival was recorded and fish were monitored for any  
625 physical or behavioral abnormalities at a range of doses. For both compounds at a dose of  
626 250 nM, survival after 4 injections was approximately 40%, and lethargy and reduced swim  
627 were observed. At 150 mM the survival increased to 65% with no evident abnormal  
628 behaviour; whereas at 50mM, the dose e adopted for the study, the survival was 85% and no  
629 evident defects were observed (**Fig. S2B**).

630

631 Optimisation of the injection procedure

632 In our pilot studies, injection of physiological solutions every other day and alternating the  
633 eye at each injection reduced fish mortality. In this way, the effect of a drug on fish  
634 survival/mortality and phenotype can be better evaluated. Therefore, all the solutions of drugs  
635 were injected in the retro-orbital veins every other day and alternating the eyes, so that each  
636 eye was injected only twice at a distance of four days.

637

638 Defining the zebrafish phenotype

639 Whole embryo phenotype following Mo and mRNA treatments were described on the basis  
640 of the following morphologic features observed under bright-field microscopy: reduced body  
641 length, curved body, reduced swimming, chorionated larvae at 4 dpf, oedema. The phenotype  
642 was assessed using a simple six points scoring system, according to the severity of that  
643 feature and where one point was normal. At least four different clutches of larvae were  
644 assessed under each of the treatment groups. Data were reported graphically as divided in two

645 groups: normal, *i.e.* embryos not showing any abnormal features, and abnormal, *i.e.* embryos  
646 showing one or more of the features described above.

647

#### 648 Cardinal vein blood velocity

649 Blood velocity was estimated in the posterior cardinal vein<sup>42</sup> by assessing frame by frame  
650 motion of single blood cells determined from video images captured in the zebrafish tail at  
651 the level of the cloaca. Four erythrocytes per fish (at least 5 embryos per group) over 10  
652 frames at video frame-rate of 30 frames per second (fps) were analyzed using ImageJ to  
653 determine mean blood cell velocity ( $\mu\text{m}\cdot\text{s}^{-1}$ ).

654

#### 655 Kaplan-Meier analysis of survival

656 Kaplan-Meier analysis was used to measure the survival of adult zebrafish or larvae  
657 following each defined treatment, using PRISM 7 software.

658

#### 659 Immunoprecipitation

660 Immunoprecipitation experiments were performed using the Pierce Classic Magnetic IP/Co-  
661 IP Kit (Thermo Fisher Scientific, San Jose, CA, cat. MAN0011737), according to  
662 manufacturer's instructions.

663

#### 664 RNA extraction and quantitative PCR

665 mRNA was extracted from embryos using column purification (RNeasy Mini Kit, Qiagen,  
666 Hilden, Germany, cat. 74104) according to the manufacturer's instructions. Working surfaces

667 were cleaned with RNase Zap (Thermo Fisher Scientific, San Jose, CA, cat. AM9780) to  
668 deactivate environmental RNase. Efficient disruption and homogenization of tissue was done  
669 using sterile RNase-free disposable pestles (Thermo Fisher Scientific, San Jose, CA, cat. 12-  
670 141-368) mounted on a cordless motor for 30 s and then passing the lysate 5-10 times  
671 through the needle (18-21 gauge) mounted on a RNase free syringe. RNA integrity was  
672 assessed on basis of 18S and 28S ribosomal RNA (rRNA) bands. mRNA was reverse  
673 transcribed into cDNA using qScript cDNA Synthesis Kit (Quanta Bio, Beverly, MA, cat.  
674 95047), Primers (IDT Technologies, Coralville, Iowa) targeting genes of interest (see **table**  
675 **S2**) and SYBR Green PCR kit (Invitrogen, Carlsbad, CA) were used for real-time qPCR, that  
676 was performed with the QuantStudio 12 k Flex system (Applied Biosystems, Foster City,  
677 CA) following the manufacturer's instructions. Gene expression was expressed as relative  
678 fold changes using the  $\Delta$ Ct method of analysis and normalized to  $\beta$ -actin.

679

#### 680 Western blotting

681 Lysates containing 20 $\mu$ g of protein each were added with Laemmli buffer (4X) and deionised  
682 water to reach a final volume of 20 $\mu$ l. A sample containing pre-stained protein standard  
683 (BioRad, Hertfordshire, UK, cat. 1610375) was used to assess molecular mass of protein  
684 bands. Samples were heated at 95°C for 5 min and loaded on a polyacrylamide gel (4-15%  
685 gradient) (BioRad, Hertfordshire, UK, cat. 4561083). Electrophoresis was performed for 30  
686 min at a voltage of 100V and then for 60 min at 150V. Gels were transferred on PVDF  
687 membranes (Amersham Hybond, Sigma-Aldrich, St Louis, MO, cat. GE10600023) for 2 h at  
688 100V. Membranes were blocked with non-fat milk 5% in PBST (PBS+0.1% Tween) for 1h at  
689 RT and probed with primary antibody overnight at 4°C. Antibodies used were: Kdm1a rabbit  
690 polyclonal (1:200, Thermo Fisher Scientific, San Jose, CA, cat. PA1-41697); anti-iNos

691 mouse monoclonal (1:200, BD Transduction Laboratories, San Jose, CA, cat. 610432); anti-  
692  $\beta$ -tubulin rabbit polyclonal (1:500, Abcam, Cambridge, UK, cat. ab6046), Anti-Histone H3  
693 nuclear marker, rabbit polyclonal (1:500, Abcam, Cambridge, UK, cat. ab1791); anti-Histone  
694 H3 (1:500, unmodified Lys4), mouse monoclonal (1:500, Merck Millipore, Massachusetts,  
695 USA, cat. 05-1341); anti-monomethyl-Histone H3 (Lys4), rabbit polyclonal (1:500, Merck  
696 Millipore, Massachusetts, USA, cat. 07-436); anti-dimethyl-Histone H3 (Lys4), rabbit  
697 monoclonal (1:500, Merck Millipore, Massachusetts, USA, cat. 04-790); anti-monomethyl-  
698 Histone H3 (Lys9), rabbit polyclonal (1:500, Merck Millipore, Massachusetts, USA, cat.  
699 ABE101); anti-dimethyl-Histone H3 (Lys9) rabbit polyclonal (1:500, Merck Millipore,  
700 Massachusetts, USA, cat. 07-212); anti-Rcor1 rabbit polyclonal (1:200, Invitrogen, Carlsbad,  
701 CA, cat. PA5-41564); anti-Hdac1 rabbit polyclonal (1:200, Abcam, Cambridge, UK, cat.  
702 ab33278); anti-Rbbp4 rabbit polyclonal (1:200, Biorbyt, Cat. orb583248); anti-Chd4 rabbit  
703 polyclonal (1:200, Biorbyt, Cambridge, UK, cat. orb575051); anti-TMT mouse monoclonal  
704 (1:200, Thermo Fisher Scientific, San Jose, CA, cat. 90075). Membranes were washed three  
705 times (5 min per wash) with PBS and incubated with HRP-conjugated goat anti-mouse  
706 (1:2000, Santa Cruz Biotechnology, Dallas, USA, SC-2005) or anti-rabbit (1:2000, Santa  
707 Cruz Biotechnology, Dallas, USA, SC-2004) antibodies for 1 h at RT. Then, membranes  
708 were washed again three times with PBS (5 min per wash). Antigen-antibody complexes  
709 were detected by incubation for 5 min to the enhanced chemiluminescence solution (ECL,  
710 Amersham) followed by exposure to a photographic film (BioMax XAR Film Kodak, Sigma-  
711 Aldrich, St Louis, MO). The film was developed and band density was quantified by  
712 densitometry using ImageJ.  $\beta$ -tubulin and Histone H3 were used as loading control for  
713 cytoplasmic and nuclear protein, respectively.

714

715

716 Sequence and structural analysis of Kdm1a protein  
717 Similarities of zebrafish and human Kdm1a proteins were assessed using Protein Blast  
718 (<https://blast.ncbi.nlm.nih.gov/Blast.cgi>). Kdm1a crystal structure was obtained from the  
719 Protein Data bank (<https://www.ebi.ac.uk/pdbe/entry/pdb/6nqm>).

720

721 Enzymatic isolation of endothelial cells from zebrafish tailfin  
722 Cells were isolated according to <sup>43</sup> with some modifications. In brief, amputated tailfin from  
723 adult Tg(*fli1*:EGFP)<sup>y1</sup> zebrafish were placed in chilled PBS, washed with calcium-free  
724 Ringer solution (116 mM NaCl, 2.6 mM KCl, and 5 mM HEPES, pH 7.0), and replaced with 1  
725 mL solution of trypsin 0.25% (Gibco) added with 50 µg collagenase P (Roche) and 1 mM  
726 EDTA. Tissue was disaggregated first using fine scissors and then by pipetting the solution  
727 with a 200-µL pipette tip every 5 min for about 30 min. Cell suspensions were filtered  
728 through a 40-µm cell strainer (BD Biosciences) into FACS tubes.

729

730 Flow cytometry characterization of *fli1*<sup>+</sup> cells from zebrafish.  
731 Cell samples were run on a BD FACS Aria (BD Biosciences). FSC-H and FSC-A were used  
732 to select cell singlets; 4',6-diamidino-2-phenylindole (DAPI) to select viable single cells;  
733 wild-type (Wik) zebrafish were used to set the gate between GFP<sup>-</sup> (*i.e.*, *fli1*<sup>-</sup>) and GFP<sup>+</sup> (*i.e.*,  
734 *fli1*<sup>+</sup>) cells. At least 10,000 of *fli1*<sup>-</sup> and *fli1*<sup>+</sup> cells (excitation [Ex]: 488 nm; emission [Em]:  
735 530 nm) were sorted into chilled PBS and 10% fetal bovine serum for further analysis.  
736 FlowJo 10 (Becton and Dickinson) was used to analyse data.

737

738 Statistical analysis



739 Results were expressed as the mean  $\pm$  SEM. Each experiment was performed 3 times  
740 (biological replicates). The Shapiro-Wilk test was used to confirm the null hypothesis that the  
741 data follow a normal distribution. Statistical comparisons between two groups or multiple  
742 groups were then performed, respectively, via Student t-test or ANOVA test using PRISM 7  
743 software followed by Bonferroni post hoc test. Log-rank test and Gehan-Breslow-Wilcoxon  
744 test were used for statistical analysis of the Kaplan-Meier curves. A P value  $<0.05$  was  
745 considered significant.

746

#### 747 Reporting summary

748 Further information on research design is available in the Nature Research Reporting  
749 Summary linked to this article.

750

#### 751 Data availability

752 TMT-labelled S-nitrosylated protein analysis mass spectrometry data have been deposited to  
753 the ProteomeXchange Consortium via the MASSIVE repository (MSV000085055) with the  
754 dataset identifier PXD017883[<https://www.ebi.ac.uk/pride/archive/projects/PXD17883>] and  
755 are freely available. Furthermore, a full list of the S-nitrosylated proteins derived from the  
756 mass-spec is included in this manuscript as Dataset S1. Gene Expression Omnibus (GEO)  
757 database, accession  
758 GSE137971[<https://www.ncbi.nlm.nih.gov/geo/query/acc.cgi?acc=GSE137971>] was used for  
759 single cell sequencing analysis. All other relevant data supporting the key findings of this  
760 study are available within the article supplementary files, and Source Data file.

761

762 **References**

- 763
- 764 1. Huber-Lang, M., Lambris, J. D. & Ward, P. A. Innate immune responses to trauma.
- 765 *Nat. Immunol.* **19**, 327–341 (2018).
- 766 2. Eming, S. A., Wynn, T. A. & Martin, P. Inflammation and metabolism in tissue repair
- 767 and regeneration. *Science (80-. )*. **356**, 1026–1030 (2017).
- 768 3. Atala, A., Irvine, D. J., Moses, M. & Shaunak, S. Wound Healing Versus
- 769 Regeneration: Role of the Tissue Environment in Regenerative Medicine. *MRS Bull.*
- 770 **35**, (2010).
- 771 4. Lee, J. *et al.* Activation of innate immunity is required for efficient nuclear
- 772 reprogramming. *Cell* **151**, 547–58 (2012).
- 773 5. Chanda, P. K. *et al.* Nuclear S-Nitrosylation Defines an Optimal Zone for Inducing
- 774 Pluripotency. *Circulation* **140**, 1081–1099 (2019).
- 775 6. Meng, S. *et al.* Transdifferentiation Requires iNOS Activation: Role of RING1A S-
- 776 Nitrosylation. *Circ. Res.* **119**, e129–e138 (2016).
- 777 7. Cooke, J. P. Therapeutic transdifferentiation: a novel approach for vascular disease.
- 778 *Circ. Res.* **112**, 748–50 (2013).
- 779 8. Akimenko, M.-A., Mari-Beffa, M., Becerra, J. & Géraudie, J. Old questions, new
- 780 tools, and some answers to the mystery of fin regeneration. *Dev. Dyn.* **226**, 190–201
- 781 (2003).
- 782 9. Hatano, E. *et al.* NF-kappaB stimulates inducible nitric oxide synthase to protect
- 783 mouse hepatocytes from TNF-alpha- and Fas-mediated apoptosis. *Gastroenterology*
- 784 **120**, 1251–62 (2001).
- 785 10. Garvey, E. P. *et al.* 1400W is a slow, tight binding, and highly selective inhibitor of
- 786 inducible nitric-oxide synthase in vitro and in vivo. *J. Biol. Chem.* **272**, 4959–63
- 787 (1997).

- 788 11. Yan, C. *et al.* Epithelial to mesenchymal transition in human skin wound healing is  
789 induced by tumor necrosis factor-alpha through bone morphogenic protein-2. *Am. J.*  
790 *Pathol.* **176**, 2247–58 (2010).
- 791 12. Asai, J. *et al.* Topical sonic hedgehog gene therapy accelerates wound healing in  
792 diabetes by enhancing endothelial progenitor cell-mediated microvascular remodeling.  
793 *Circulation* **113**, 2413–24 (2006).
- 794 13. Shi, Y. *et al.* Histone Demethylation Mediated by the Nuclear Amine Oxidase  
795 Homolog LSD1. *Cell* **119**, 941–953 (2004).
- 796 14. Forneris, F., Binda, C., Vanoni, M. A., Mattevi, A. & Battaglioli, E. Histone  
797 demethylation catalysed by LSD1 is a flavin-dependent oxidative process. *FEBS Lett.*  
798 **579**, 2203–7 (2005).
- 799 15. Ballas, N. *et al.* Regulation of neuronal traits by a novel transcriptional complex.  
800 *Neuron* **31**, 353–65 (2001).
- 801 16. Wang, Y. *et al.* LSD1 is a subunit of the NuRD complex and targets the metastasis  
802 programs in breast cancer. *Cell* **138**, 660–72 (2009).
- 803 17. Metzger, E. *et al.* LSD1 demethylates repressive histone marks to promote androgen-  
804 receptor-dependent transcription. *Nature* **437**, 436–9 (2005).
- 805 18. Wissmann, M. *et al.* Cooperative demethylation by JMJD2C and LSD1 promotes  
806 androgen receptor-dependent gene expression. *Nat. Cell Biol.* **9**, 347–53 (2007).
- 807 19. Huang, J. *et al.* p53 is regulated by the lysine demethylase LSD1. *Nature* **449**, 105–8  
808 (2007).
- 809 20. Wang, J. *et al.* The lysine demethylase LSD1 (KDM1) is required for maintenance of  
810 global DNA methylation. *Nat. Genet.* **41**, 125–9 (2009).
- 811 21. Kontaki, H. & Talianidis, I. Lysine methylation regulates E2F1-induced cell death.  
812 *Mol. Cell* **39**, 152–60 (2010).

- 813 22. Tan, A. H. Y. *et al.* Lysine-Specific Histone Demethylase 1A Regulates Macrophage  
814 Polarization and Checkpoint Molecules in the Tumor Microenvironment of Triple-  
815 Negative Breast Cancer. *Front. Immunol.* **10**, (2019).
- 816 23. Hou, Y. *et al.* Cellular diversity of the regenerating caudal fin. *Sci. Adv.* **6**, eaba2084  
817 (2020).
- 818 24. Xu, C. *et al.* Arteries are formed by vein-derived endothelial tip cells. *Nat. Commun.* **5**,  
819 5758 (2014).
- 820 25. Cristina de Assis, M., Cristina Plotkowski, M., Fierro, I. M., Barja-Fidalgo, C. & de  
821 Freitas, M. S. Expression of inducible nitric oxide synthase in human umbilical vein  
822 endothelial cells during primary culture. *Nitric oxide Biol. Chem.* **7**, 254–61 (2002).
- 823 26. Bill, B. R., Petzold, A. M., Clark, K. J., Schimmenti, L. A. & Ekker, S. C. A primer for  
824 morpholino use in zebrafish. *Zebrafish* **6**, 69–77 (2009).
- 825 27. Stainier, D. Y. R. *et al.* Guidelines for morpholino use in zebrafish. *PLOS Genet.* **13**,  
826 e1007000 (2017).
- 827 28. Takeuchi, M. *et al.* LSD1/KDM1A promotes hematopoietic commitment of  
828 hemangioblasts through downregulation of Etv2. *Proc. Natl. Acad. Sci. U. S. A.* **112**,  
829 13922–7 (2015).
- 830 29. Xie, Q. W., Kashiwabara, Y. & Nathan, C. Role of transcription factor NF-kappa  
831 B/Rel in induction of nitric oxide synthase. *J. Biol. Chem.* **269**, 4705–8 (1994).
- 832 30. Hess, D. T., Matsumoto, A., Kim, S.-O., Marshall, H. E. & Stamler, J. S. Protein S-  
833 nitrosylation: purview and parameters. *Nat. Rev. Mol. Cell Biol.* **6**, 150–66 (2005).
- 834 31. Saleque, S., Kim, J., Rooke, H. M. & Orkin, S. H. Epigenetic Regulation of  
835 Hematopoietic Differentiation by Gfi-1 and Gfi-1b Is Mediated by the Cofactors  
836 CoREST and LSD1. *Mol. Cell* **27**, (2007).
- 837 32. Hu, X. *et al.* LSD1-mediated epigenetic modification is required for TAL1 function

- 838 and hematopoiesis. *Proc. Natl. Acad. Sci.* **106**, (2009).
- 839 33. Sprüssel, A. *et al.* Lysine-specific demethylase 1 restricts hematopoietic progenitor  
840 proliferation and is essential for terminal differentiation. *Leukemia* **26**, (2012).
- 841 34. Kerényi, M. A. *et al.* Histone demethylase Lsd1 represses hematopoietic stem and  
842 progenitor cell signatures during blood cell maturation. *Elife* **2**, (2013).
- 843 35. Fu, D.-J., Li, J. & Yu, B. Annual review of LSD1/KDM1A inhibitors in 2020. *Eur. J.*  
844 *Med. Chem.* **214**, 113254 (2021).
- 845 36. Yik, J. H. N. *et al.* Inhibition of P-TEFb (CDK9/Cyclin T) kinase and RNA  
846 polymerase II transcription by the coordinated actions of HEXIM1 and 7SK snRNA.  
847 *Mol. Cell* **12**, 971–82 (2003).
- 848 37. Foster, M. W., Hess, D. T. & Stamler, J. S. Protein S-nitrosylation in health and  
849 disease: a current perspective. *Trends Mol. Med.* **15**, 391–404 (2009).
- 850 38. Hayashi, S., Tamura, K. & Yokoyama, H. Chromatin dynamics underlying the precise  
851 regeneration of a vertebrate limb - Epigenetic regulation and cellular memory. *Semin.*  
852 *Cell Dev. Biol.* **97**, 16–25 (2020).
- 853 39. Poss, K. D., Shen, J. & Keating, M. T. Induction of *lef1* during zebrafish fin  
854 regeneration. *Dev. Dyn.* **219**, 282–6 (2000).
- 855 40. Petrie, T. A. *et al.* Macrophages modulate adult zebrafish tail fin regeneration.  
856 *Development* **141**, 2581–91 (2014).
- 857 41. Pugach, E. K., Li, P., White, R. & Zon, L. Retro-orbital injection in adult zebrafish. *J.*  
858 *Vis. Exp.* (2009). doi:10.3791/1645
- 859 42. Rider, S. A. *et al.* Techniques for the in vivo assessment of cardio-renal function in  
860 zebrafish (*Danio rerio*) larvae. *J. Physiol.* **590**, 1803–9 (2012).
- 861 43. Matrone, G. *et al.* Fli1 + cells transcriptional analysis reveals an Lmo2–Prdm16 axis in  
862 angiogenesis. *Proc. Natl. Acad. Sci.* **118**, e2008559118 (2021).

863 **Acknowledgements**

864 This project has received funding from the European Union's Horizon 2020 research and  
865 innovation programme under the Marie Skłodowska-Curie grant agreement n. 797304 (to  
866 G.M.). This work was also supported by the British Heart Foundation (BHF) CoRE Award  
867 (RE/13/3/30183) and Transition Fellowship (RE/18/5/34216) (to G.M.); the BHF Chair of  
868 Translational Cardiovascular Sciences (CH/11/2/28733) and Centre for Regenerative  
869 Medicine (RM/17/3/33381) (to A.H.B.); the Cullen Trust for Health Care (to J.P.C. and  
870 G.M.); and the National Institutes of Health R01 Grants HL 148338 and HL133254 (to  
871 J.P.C.). Furthermore, we are grateful to David E. Newby, supported by the British Heart  
872 Foundation awards CH/09/002, RG/16/10/32375, RE/18/5/34216) and the Wellcome Trust  
873 award WT103782AIA, for providing additional funding support. We thank John F. Rawls lab  
874 (Duke University School of Medicine) for providing *Tg(nfkb:EGFP)<sup>nc1</sup>* zebrafish.

875 **Author information**

876 Author contributions

877 G.M. is the senior author of this work and is primarily responsible for the conception, design  
878 and experimental investigation, data collection and analysis, resources, and original and  
879 revised drafts; S.Y.J., J.M.C., A.J. and H.E.L. contributed to mass spectrometry run and  
880 dataset collection; C.C., K.R. and JR contributed to bioinformatic analysis; M.D. and A.H.B  
881 contributed resources, advised on experimental design and contributed to manuscript editing  
882 and discussions; J.P.C. contributed to conceptualization, resources and editing.

883 **Ethics declarations**

884 Competing interests

885 The authors declare no competing interests.

886

887 **Legends**

888 **Figure 1 – Modulation of Nos and nuclear protein S-nitrosylation during tailfin**

889 **regeneration in adult zebrafish. A.** Real time PCR for *nos1*, *nos2a* and *nos2b* in tailfin at 3,  
890 5, 10 dpa. **B.** Western blot (WB) analysis of Nos2 in tailfins at 3, 5 and 10 dpa and semi-  
891 quantitative analysis of bands. **C.** WB analysis of Nos2 in nucleus and cytoplasm of tailfins at  
892 3, 5 and 10 dpa. Semi-quantitative analysis of bands shows nuclear to cytoplasmic protein  
893 ratio. **D.** WB analysis of S-nitrosylated nuclear proteins in the regenerating tailfin. S-  
894 nitrosothiols were specifically labelled with TMT. An anti-TMT antibody was used to detect  
895 S-nitrosylated proteins. Neg and Pos are respectively the negative (without ascorbic acid) and  
896 positive (with S-nitrosoglutathione) controls. **E-F.** WB analysis of S-nitrosylated nuclear  
897 proteins in tailfin following treatment with L-NAME 10 or 50 mM, 2-Phenyl-4,4,5,5-  
898 tetramethyl imidazoline-1-oxyl 3-oxide (PTIO) 3 or 10 mM, S-Nitroso-N-acetyl-DL-  
899 penicillamine (SNAP) 10 or 30 mM, or PBS (control). The dot plot shows changes in tailfin  
900 regeneration rate, here shown at 7 dpa, following drug treatments compared to control.  $\beta$ -  
901 tubulin was used as loading control for total or cytoplasmic proteins. Histone H3 was used as  
902 loading control for nuclear proteins. Dpa – days post-amputation. N=3 biological replicates,  
903 one way ANOVA test followed by Bonferroni's multiple comparisons test was used to  
904 compare the means, p values shown are vs uninjured or control, all other comparisons are not  
905 significant. Data are presented as mean values +/- SEM.

906 **Figure 2 – Bioinformatic analysis of the S-nitrosylome in zebrafish tailfin regeneration.**

907 **A.** Workflow for the analysis of the S-nitrosylome. Tailfins of zebrafish (6 months old) were  
908 amputated; regrown tissue was collected in uninjured and at 3, 5 and 10 dpa (dash red lines  
909 represent the edge of the amputation); nuclear proteins were extracted and labelled with  
910 iodoTMT, digested with trypsin, and S-nitroso-peptides enriched through anti-TMT antibody  
911 containing resin and followed by LC-MS-MS. **B-C.** Hierarchical clustering heat map and

912 Venn diagram showing the dynamic changes in the number of S-nitrosylated nuclear proteins  
913 during the regeneration compared to uninjured. **D.** Hallmark pathways enrichment by the  
914 differentially expressed S-nitrosylated proteins during regeneration compared to uninjured.  
915 The significant pathways are displayed along the x-axis. Dpa - day post-amputation. N=2  
916 biological replicates, followed by bioinformatic analysis.

917 **Figure 3 – Role of S-nitrosylation of Kdm1a in tailfin regeneration in adult zebrafish. A.**  
918 MS/MS fragmentation spectrum for the Cys334-containing peptide of Kdm1a. Peptide  
919 sequence is shown at the top left of the spectrum, with the annotation of the identified  
920 matched amino terminus-containing ions (b ions) in black and the carboxyl terminus-  
921 containing ions (y ions) in red. The spectrum confirms the identity of the peptides CPLYEAN  
922 and the labeled C as S-nitrosylated cysteine. **B.** Line graph reporting the quantification of  
923 Kdm1a S-nitrosylation (normalized by total Kdm1a) and Kdm1a activity during tailfin  
924 regeneration. **C.** Western blotting (WB) for S-nitrosylated Kdm1a in uninjured and at 3, 5  
925 and 10 dpa. Samples were previously immunoprecipitated (IP) for Kdm1a. IP with IgG and  
926 input were used as controls. **D-E-F.** WB for Kdm1a, CoRest and NuRD complexes  
927 components following IP with Kdm1a antibody in tailfin uninjured or injured at 5 dpa. Dpa –  
928 days post-amputation. N=3 biological replicates.

929 **Figure 4 – Effects of *kdm1a* knockdown in adult zebrafish. A.** Western blotting (WB)  
930 analysis of Kdm1a control and morpholino KD. Dot plot shows semiquantitative analysis of  
931 bands. Two-tailed t-test. **B.** Effects of *Kdm1a* KD on tailfin regeneration. Dashed red line  
932 represents the edge of the resection. Scale bar indicates 2 mm. **C.** Line graph showing  
933 changes in tailfin regeneration rate following *kdm1a* KD. Two-way ANOVA followed by  
934 Bonferroni's multiple comparisons test. **D-E.** WB for H3K4unme (unmethylated), H3K4me1,  
935 H3K4me2 and H3K4me3 in control uninjured, injured and injured + *kdm1a* KD at at 5 dpa.



936 Dot plot shows semi-quantitative analysis of bands. Histone H3 was used as loading control.  
937 Dpa - days post-amputation. Two-way ANOVA followed by Bonferroni's multiple  
938 comparisons test, p values indicate comparisons of uninjured vs other groups. N=3 biological  
939 replicates. Data are presented as mean values +/- SEM.

940 **Figure 5 – Analysis of S-nitrosylation in endothelial cells during tailfin regeneration. A.**

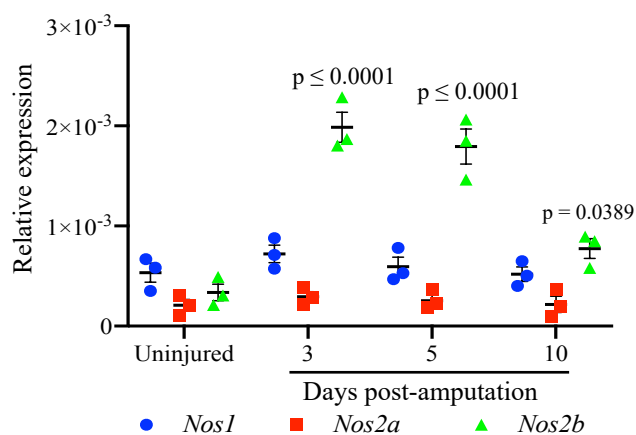
941 Brightfield and fluorescence images of *Tg(fli1:EGFP)<sup>y1</sup>* zebrafish tailfin at 3 days post-  
942 amputation (dpa) showing formation of new vessel branches (GFP signal). Scale bar  
943 measures 500  $\mu$ m. **B.** FACS plot of GFP<sup>+</sup> and GFP<sup>-</sup> cells in the tailfin in control and during  
944 regeneration were separated by FACS. **C.** Quantification of GFP<sup>+</sup> cells as shown in FACS  
945 plots. Two-tailed t-test. **D.** Western blotting (WB) of total S-nitrosylated proteins in zebrafish  
946 tailfin endothelial (GFP<sup>+</sup>) cells. **E.** WB of Kdm1a and S-nitrosylated Kdm1a in endothelial  
947 (GFP<sup>+</sup>) cells control, injury and injury + PTIO (NO scavenger) 10 mM. Dot plot shows semi-  
948 quantitative analysis. p values vs 5 dpa group. **F.** Vessel density analysis in *Tg(fli1:EGFP)<sup>y1</sup>*  
949 zebrafish tailfin uninjured, injured and injured + PTIO 10 mM, measured as total length of  
950 vessels. **G.** ChIP-PCR analysis in GFP<sup>+</sup> cells isolated from the regenerating tailfin showing  
951 H3K4me2-binding complex with *vegfaa* and *tek* promoters. Rabbit IgG were used as a  
952 negative control. **H.** Real time PCR analysis for endothelial genes in GFP<sup>+</sup> cells from  
953 zebrafish control, injury and injury + PTIO 10 mM. Histone H3 was used as loading control.  
954 One-way ANOVA followed by Bonferroni's multiple comparisons test, p values indicate  
955 comparisons vs uninjured. N=3 biological replicates. Data are presented as mean values +/-  
956 SEM.

957 **Figure 6. Modulation of Kdm1a S-nitrosylation during tailfin regeneration. A.** *Kdm1a*

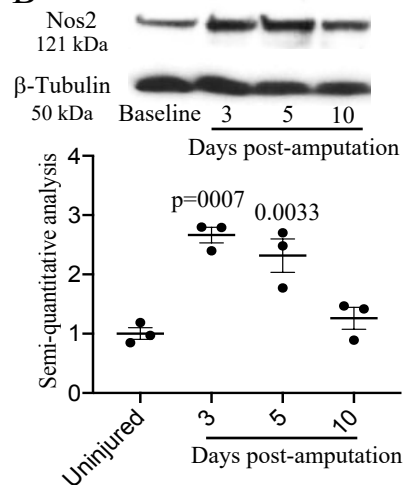
958 mRNA C334A was generated by site-directed mutagenesis, replacing the aa Cys334 with  
959 Ala. B-D. Zebrafish embryos injected with *kdm1a* morpholino (Mo), or co-injected with

960 *kdm1a* Mo with *kdm1a* mRNA C334A or wild type. **B.** Western blotting and semi-  
961 quantitative analysis showed the effective knockdown and rescue of *kdm1a* following the  
962 different treatments.  $\beta$ -tubulin was used as loading control. **C-D.** Images and dot plot of  
963 tailfin regeneration following *kdm1a* modulation (P values vs control). Scale bar measures  
964 100  $\mu$ m. **E.** Working model. Tissue injury promotes the S-nitrosylation of the Cys334 of  
965 Kdm1a. S-nitrosylated Kdm1a detaches from the CoRest complex and loses its demethylase  
966 activity on H3K4. One-way ANOVA followed by Bonferroni's multiple comparisons test, p  
967 values indicate comparisons vs control. N=3 biological replicates. Data are presented as mean  
968 values +/- SEM.

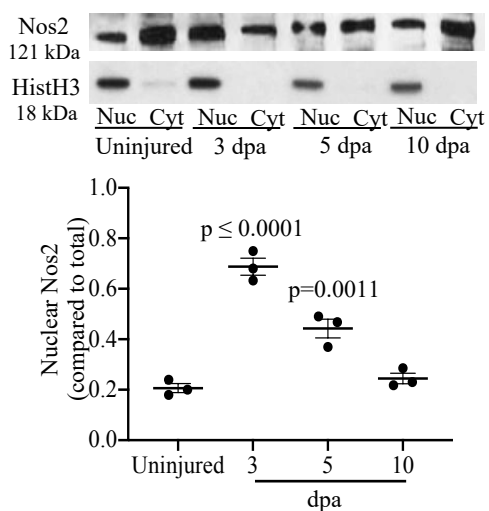
**A**



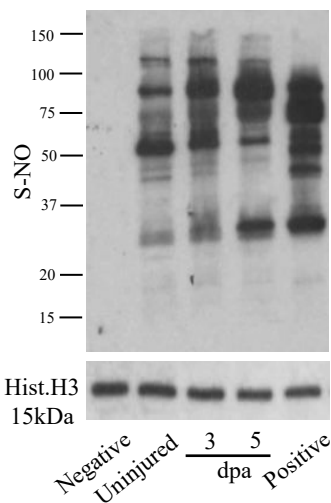
**B**



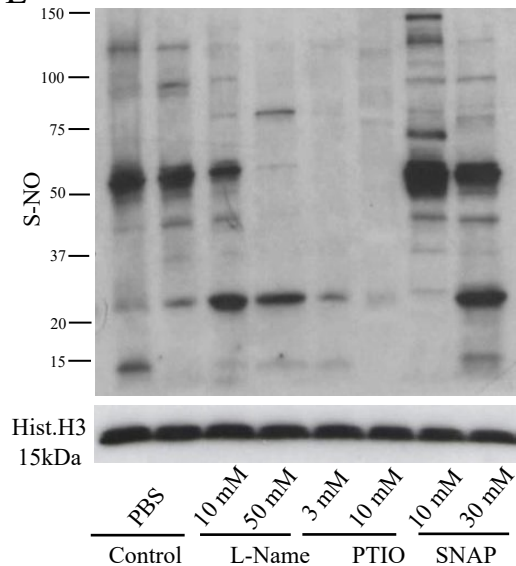
**C**



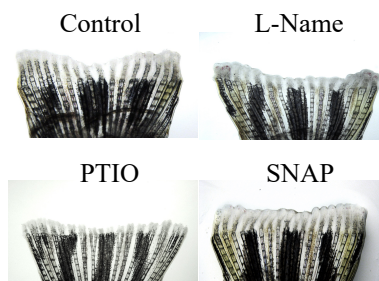
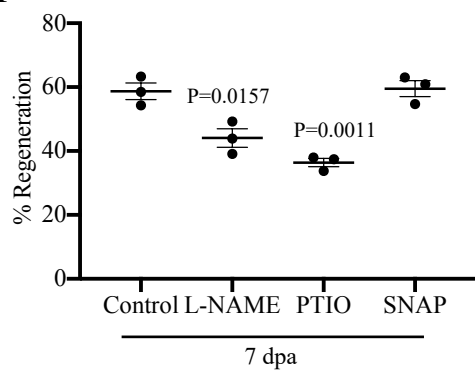
**D**

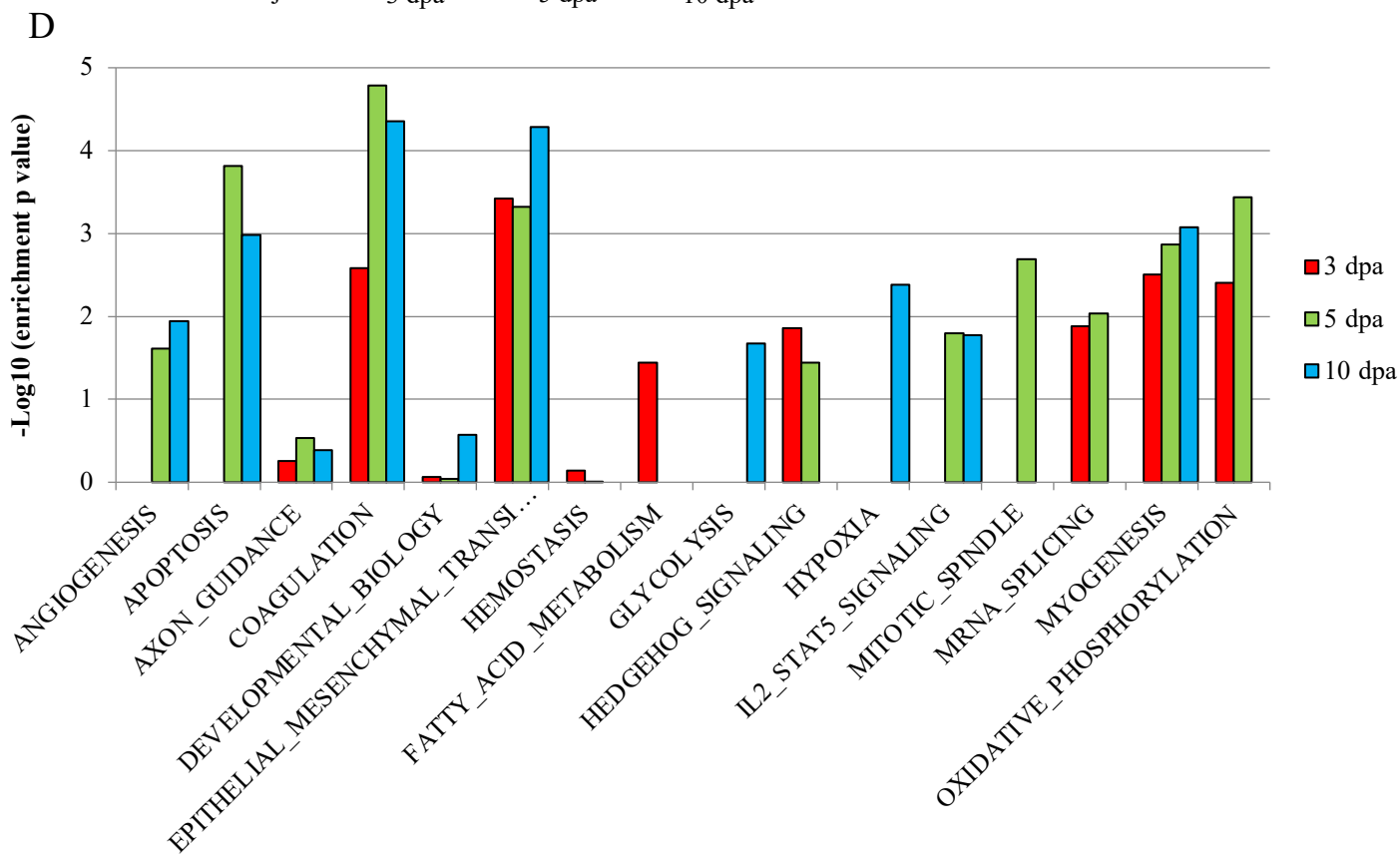
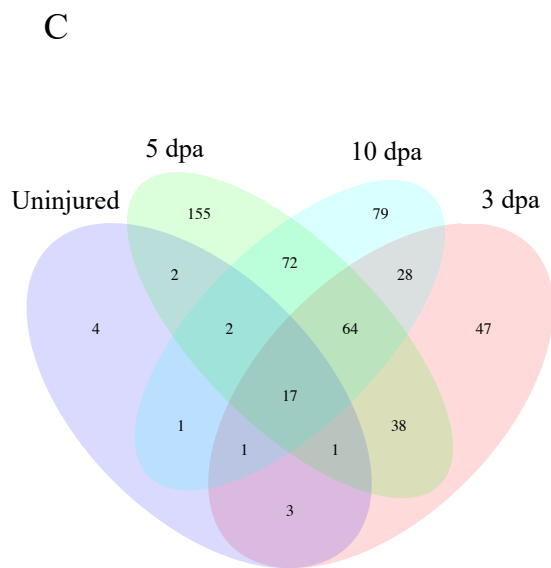
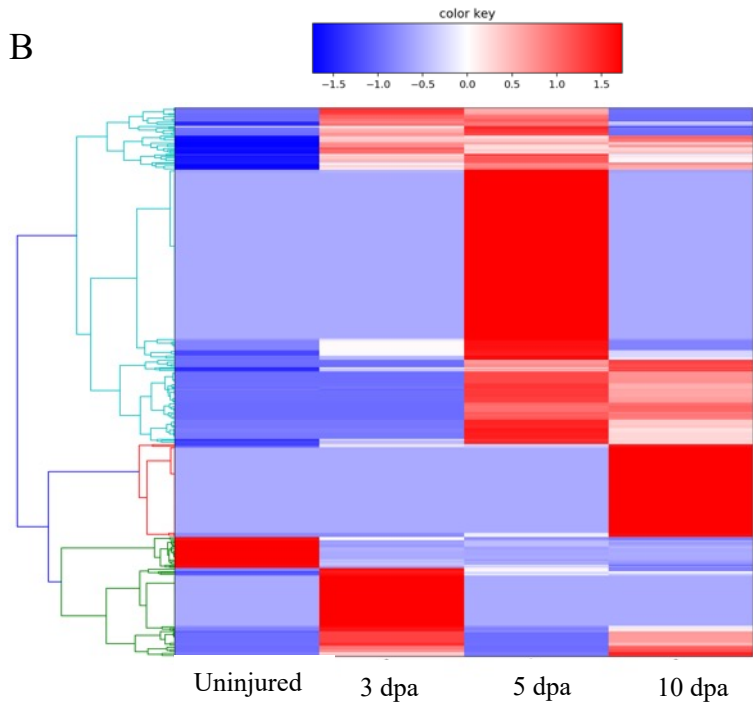
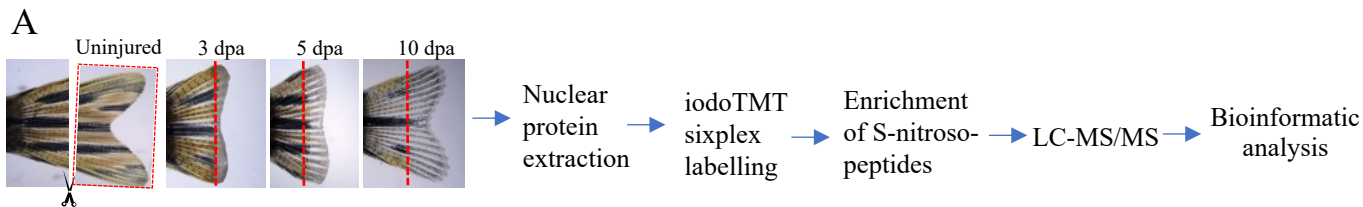


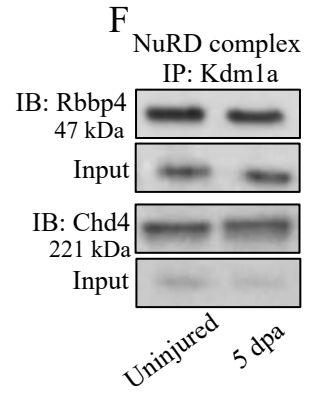
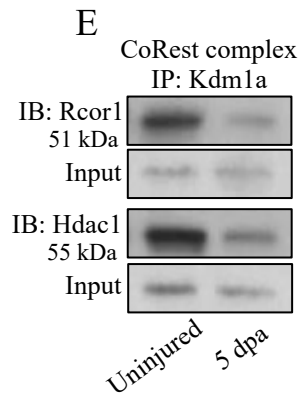
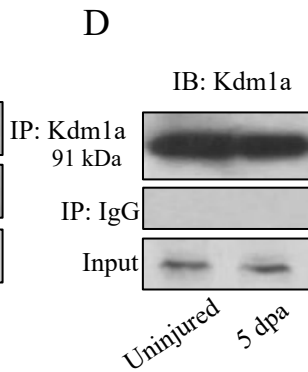
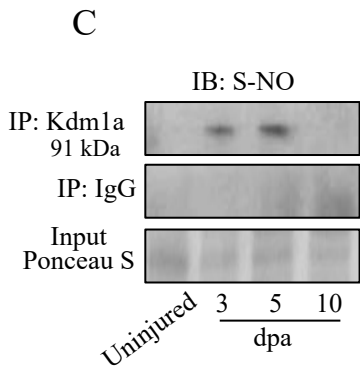
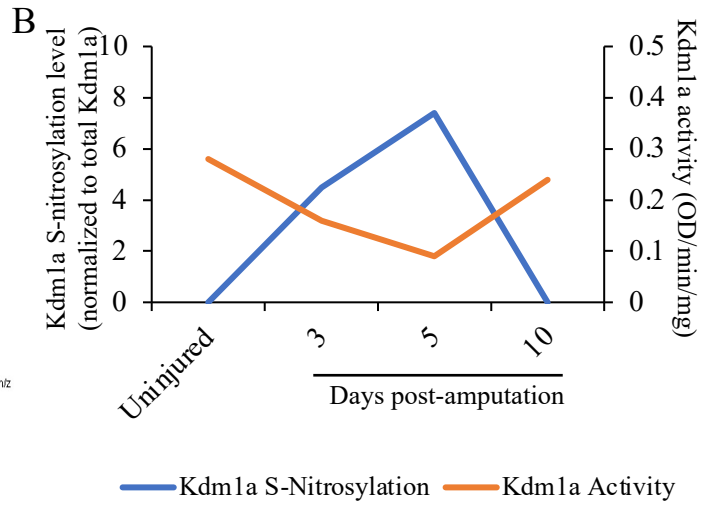
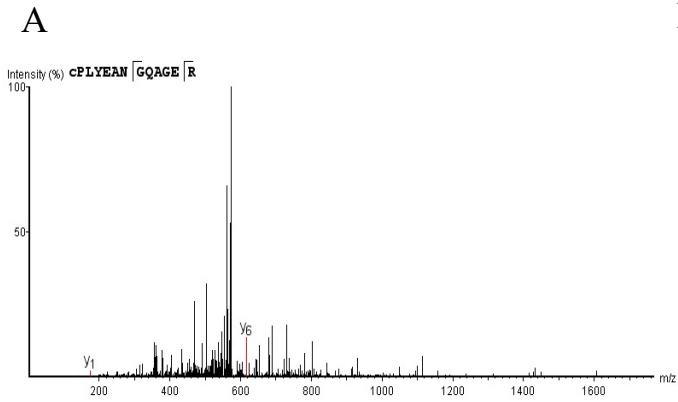
**E**



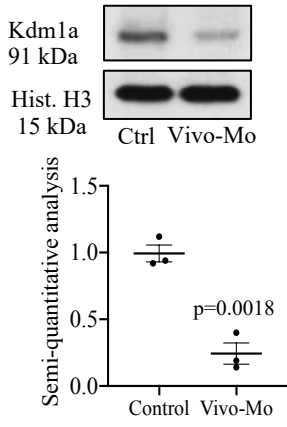
**F**



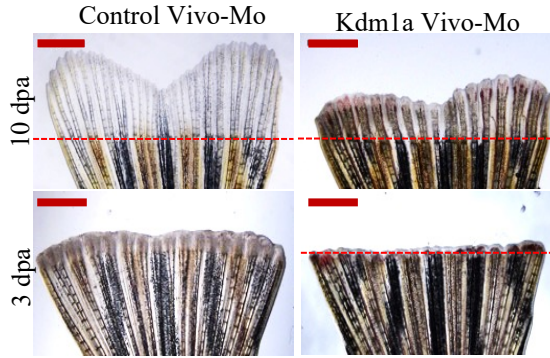




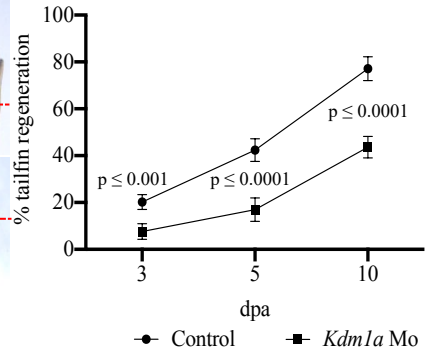
A



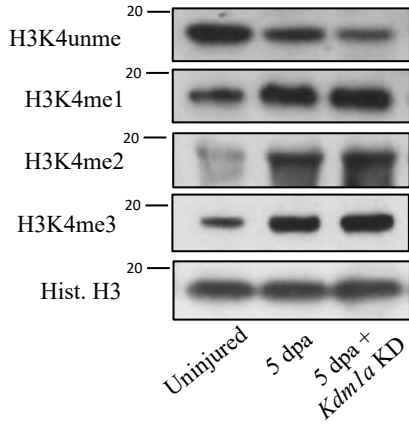
B



C



D



E

